Pergamon

Int. J. Heat Mass Transfer. Vol. 41, No. 11, pp. 1417–1435, 1998

Printed in Great Britain
0017–9310/98 $19.00+0.00

PII: S0017–9310(97)00265–2

Transitions and chaos for free convection in a rotating porous layer

PETER VADASZ†
Department of Mechanical Engineering, University of Durban-Westville Private Bag X54001, Durban 4000, South Africa

and

SHMUEL OLEK
Research and Development Division, Israel Electric Corporation, P.O. Box 10, Haifa 31000, Israel

(*Received* 22 *May* 1997 *and in final form* 27 *August* 1997)

Abstract—The non-linearity which is inherently present in centrifugally driven free convection in porous media raises the problem of multiple solutions existent in this particular type of system. The solution to the non-linear problem is obtained by using a truncated Galerkin method to obtain a set of ordinary differential equation for the time evolution of the Galerkin amplitudes. It is demonstrated that Darcy's model when extended to include the time derivative term yields, subject to appropriate scaling, the familiar Lorenz equations although with different coefficients, at a similar level of Galerkin truncation. The system of ordinary differential equations was solved by using Adomian's decomposition method. Below a certain critical value of the centrifugally related Rayleigh number the obvious unique motionless conduction solution is obtained. At slightly super-critical values of the centrifugal Rayleigh number a pitchfork bifurcation occurs, leading to two different steady solutions. For highly supercritical Rayleigh numbers transition to chaotic solutions occurs via a Hopf bifurcation. The effect of the time derivative term in Darcy's equation is shown to be crucial in this truncated model as the value of Rayleigh number when transition to the non-periodic regime occurs goes to infinity at the same rate as the time derivative term goes to zero. Examples of different convection solutions and the resulting rate of heat transfer are provided.

1. INTRODUCTION

Transport phenomena in rotating porous media have a variety of applications in engineering. The effect of rotation and of free convection as a result of the centrifugal body force is of particular interest from both the practical and theoretical points of view.

Engineering applications include among others, the food, chemical and materials processing industries and rotating machinery. The problem of solidification of binary alloys includes also transport phenomena in rotating porous media as the dendritic mushy zone is regarded for all practical purposes as a porous medium. Other applications of the porous medium approach are discussed by Nield and Bejan [1] and Bejan [2] in comprehensive reviews of the fundamentals of heat convection in porous media. Bejan [2] mentions among the applications of heat transfer in porous media the process of cooling of winding structures in high-power density electric machines. When this applies to a rotor of an electric machine, say generator (or motor), rotation effects become relevant as well.

Research results (Patil and Vaidyanathan [3], Jou and Liaw [4, 5], Rudraiah, Shivakumara and Friedrich [6] and Palm and Tyvand [7]) are available for free convection in rotating porous media resulting from gravity in the presence of a single fluid or binary mixture. However, for a rotating porous matrix, the additional centrifugal body force has to be considered. This force generates free convection in the same manner as the gravity force causes natural convection. Vadasz [8] presented an analytical solution to the three-dimensional free convection problem in a long rotating porous box for the case when the temperature gradient resulting from the imposed conditions on the boundary is perpendicular to the centrifugal body force. The analysis focused on the effect of the Coriolis force on the basic free convection solution, for high values of Ekman number. Secondary circulation was obtained in a plane perpendicular to the leading free convection plane as a result of the Coriolis effect on the flow. Analytical solutions for the linear stability of free convection in a porous layer subject to rotation for the case when the temperature gradient resulting from the conditions imposed on the boundaries is collinear with the centrifugal body force were presented by Vadasz [9] considering a porous layer which is placed an arbitrary positive distance from the axis

† Author to whom correspondence should be addressed.

NOMENCLATURE

Da	Darcy number, defined by k_*/L_*^2
$\hat{\mathbf{e}}_x$	unit vector in the x direction
$\hat{\mathbf{e}}_y$	unit vector in the y direction
$\hat{\mathbf{e}}_z$	unit vector in the z direction
$\hat{\mathbf{e}}_n$	unit vector in the normal to the boundary, positive outwards
H_*	the height of the layer
H	the front aspect ratio of the porous layer, equals H_*/L_*
k_*	permeability of the porous domain
L_*	the length of the porous layer
M_f	a ratio between the heat capacity of the fluid and the effective heat capacity of the porous domain
p	reduced pressure generalised to include the constant component of the centrifugal term (dimensionless)
Pr	Prandtl number, equals ν_*/α_{e*}
$\mathbf{q}$	dimensionless filtration velocity vector, equals $u\hat{\mathbf{e}}_x + v\hat{\mathbf{e}}_y + w\hat{\mathbf{e}}_z$
R	scaled centrifugal Rayleigh number, equals $(Ra_\omega + Ra_{\omega 0}/2)H^2/\pi^2(H^2+1)^2$
Ra_ω	porous media centrifugal Rayleigh number related to the contribution of the horizontal location within the porous layer to the centrifugal acceleration, equals $\beta_* \Delta T_c \omega_*^2 L_*^2 k_* M_f/\alpha_{e*}\nu_*$
$Ra_{\omega 0}$	porous media centrifugal Rayleigh number related to the contribution of the offset distance from the rotation axis to the centrifugal acceleration, equals $\beta_* \Delta T_c \omega_*^2 x_{0*} L_* k_* M_f/\alpha_{e*}\nu_*$
T	dimensionless temperature, equals $(T_* - T_C)/(T_H - T_C)$
T_C	coldest wall temperature
T_H	hottest wall temperature
u	horizontal x component of the filtration velocity
v	horizontal y component of the filtration velocity
w	vertical component of the filtration velocity
W_*	the width of the layer
W	the top aspect ratio of the porous layer, equals W_*/L_*
x_0	the dimensionless offset distance from the rotation axis, equals x_*/L_*
x	horizontal length coordinate
y	horizontal width coordinate
z	vertical coordinate
X	rescaled amplitude A_{11}, equation (18)
Y	rescaled amplitude B_{11}, equation (18)
Z	rescaled amplitude B_{20}, equation (18).

Greek symbols

α	a parameter related to the time derivative term in Darcy's equation
α_{e*}	effective thermal diffusivity
β_*	thermal expansion coefficient
γ	a parameter defined by equation (17)
ΔT_c	characteristic temperature difference
θ	a parameter, defined by equation (12)
μ_*	fluid's dynamic viscosity
ν_*	fluid's kinematic viscosity
ξ	a parameter, defined by equation (12)
τ	rescaled time, defined by equation (12)
ϕ	porosity
χ	a coefficient of the time derivative term in Darcy's equation, equals $\phi Pr/Da$
ψ	stream function
ω_*	angular velocity of the rotating box.

Subscripts

*	dimensional values
c	characteristic values
C	related to the coldest wall
cr	critical values
H	related to the hottest wall.

of rotation. The linear stability analysis provided the stability criteria, i.e., the critical centrifugal Rayleigh numbers, the critical wave numbers and the corresponding eigenfunctions for different values of the parameter controlling the offset distance from the axis of rotation, and allowed to describe qualitatively the convective flow. However, as usual, the linear stability analysis cannot provide information regarding the values of the convection amplitudes nor regarding the average rate of heat transfer. The objective of the present paper is to report the results of non-linear solutions to this problem including possible transitions between different regimes of convection at supercritical values of the centrifugal Rayleigh number. This is accomplished by adopting Adomian's decomposition method (Adomian [10, 11]) to solve the set of ordinary differential equations obtained via a truncated Galerkin expansion. Adomian's decomposition method was shown to provide extremely accurate results for a wide range of non-linear problems (see Olek [12, 13]), some of which have closed form analytical solutions and the comparison between the decomposition method and the known analytical (or alternatively numerical) results as presented by Olek [12, 13] agreed up to 14 significant digits.

The objective of the present paper is to demonstrate the possible convection regimes at supercritical values of the centrifugal Rayleigh number and evaluate the corresponding average rate of heat transfer for the problem of centrifugally driven convection in a porous layer placed an arbitrary positive distance from the axis of rotation.

2. PROBLEM FORMULATION

A narrow fluid saturated porous layer subject to rotation is placed a dimensionless distance x_0 from the axis of rotation as presented in Fig. 1. The offset distance is presented in a dimensionless form representing the ratio between the dimensional offset distance and the length of the porous layer in the form $x_0 = x_{0*}/L_*$. Two systems of coordinates are presented in Fig. 1, the first (x', y', z') is linked to the axis of rotation and the second (x, y, z), placed a horizontal distance x_0 apart from the first one, belongs to the porous layer coordinates. A positive temperature gradient in the x direction is anticipated as a result of the imposed thermal boundary conditions. This temperature gradient is collinear with the centrifugal acceleration. The significance of the variation of the centrifugal acceleration in the x direction depends on the offset distance from the axis of rotation. For the layer which is adjacent to the rotation axis (i.e., $x_0 = 0$) the variation of the centrifugal acceleration leads practically to a zero acceleration at $x = 0$ and a maximum value of acceleration at $x = 1$. However, for the layer which is far away from the rotation axis ($x_0 \gg 1$) the centrifugal acceleration is almost constant resembling the problem of a porous layer heated from below subject to gravity (here 'below' means the location where $x = 1$). The front aspect ratio of the layer is defined as $H = H_*/L_*$ where H_* and L_* are the height and the length of the layer, respectively. The top aspect ratio is $W = W_*/L_*$ where W_* is the width of the layer. The following analysis is confined to a narrow layer, i.e. $W \ll 1$. Free convection may occur as a result of the centrifugal body force while the gravity force is neglected. The condition for this assumption to be valid was developed by Vadasz [9]. In addition Govender [14] showed that in the corresponding problem of combined gravity and centrifugal buoyancy the linear stability results, i.e. the critical values and the eigen-functions are identical to the problem where gravity effects are weak and therefore neglected. Two inertial effects are considered. The first is the centrifugal acceleration, as far as changes in density are concerned and the second is the time derivative term in Darcy's equation. Other than that Darcy's law is assumed to govern the fluid flow (extended to include the centrifugal acceleration), while the Boussinesq approximation is applied for the effects of density variations. As a narrow layer is considered, i.e. $W \ll 1$, a Cartesian coordinate system can be used and the component of the centrifugal acceleration in the y direction can be neglected (see Vadasz [9]). Under these conditions the following dimensionless set of governing equations is obtained (see Vadasz [9] for the derivation of equation (2) without the time derivative term, and Dagan [15] for the derivation of equations (1) and (3))

$$\nabla \cdot \mathbf{q} = 0 \tag{1}$$

$$\left[\frac{1}{\chi}\frac{\partial}{\partial t} + 1\right]\mathbf{q} = -\nabla p - [Ra_{\omega 0} + Ra_{\omega} x]T\hat{\mathbf{e}}_x \tag{2}$$

$$\frac{\partial T}{\partial t} + \mathbf{q} \cdot \nabla T = \nabla^2 T \tag{3}$$

Equations (1)–(3) are presented in a dimensionless

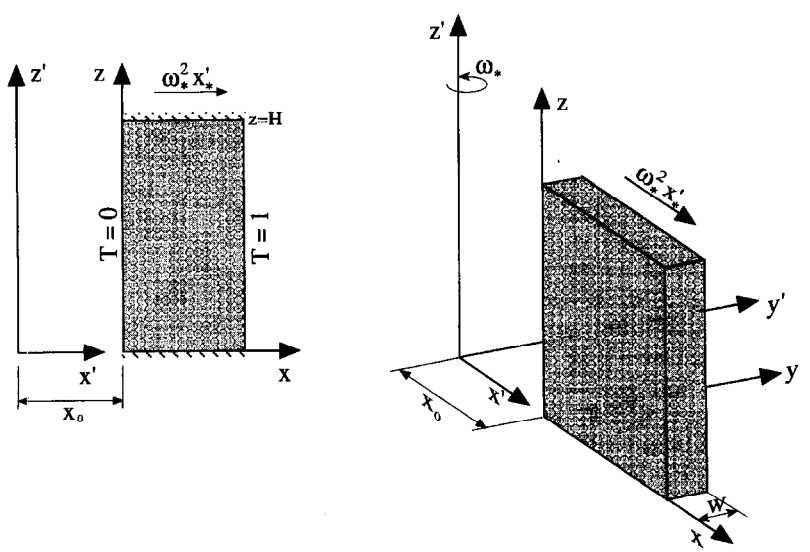

Fig. 1. A rotating fluid saturated porous layer distant from the centre of rotation and subject to different temperatures at the sidewalls.

form. The values $\alpha_{e^*}/L_* M_f$, $\mu_* \alpha_{e^*}/k_* M_f$, and $\Delta T_c = (T_H - T_C)$ are used to scale the filtration velocity components (u_*, v_*, w_*), pressure (p_*), and temperature variations $(T_* - T_C)$, respectively, where α_{e^*} is the effective thermal diffusivity, μ_* is fluid's viscosity, k_* is the permeability of the porous matrix and M_f is the ratio between the heat capacity of the fluid and the effective heat capacity of the porous domain. The length of the layer L_* was used for scaling the variables x_*, y_*, z_* and L_*^2/α_{e^*} for scaling the time t_*. Accordingly, $x = x_*/L_*$, $y = y_*/L_*$ and $z = z_*/L_*$ and $t = t_* \alpha_{e^*}/L_*^2$. In equation (2) one observes two different centrifugal Rayleigh numbers; $Ra_{\omega 0} = \beta_* \Delta T_c \omega_*^2 x_{0^*} L_* k_* M_f/\alpha_{e^*} \nu_*$ is the centrifugal Rayleigh number representing the contribution of the offset distance from the rotation axis to the centrifugal acceleration and $Ra_\omega = \beta_* \Delta T_c \omega_*^2 L_*^2 k_* M_f/\alpha_{e^*} \nu_*$ represents the contribution of the horizontal location within the porous layer to the centrifugal acceleration. The time derivative term was included in Darcy's equation (2), where χ is a dimensionless group which includes the Prandtl and Darcy numbers as well as the porosity of the porous domain and is defined by $\chi = \phi\, Pr/Da$. It is only through this combined dimensionless group that the Prandtl number is affecting the flow in porous media. Hence, while Pr can take values from as small as 10^{-3} for liquid metals and up to 10^3 for oils, the corresponding values of χ will be magnified by a factor of ϕ/Da which is typically a big number. This factor can take values from 10 to 10^{20}. Therefore the values of χ can be expected in the range from 10^{-2} to 10^{23}. Typical values of χ are quite big, a fact which provides the justification for neglecting the time derivative term in Darcy's equation. However, there are circumstances when its value can become of a unit order of magnitude or even smaller, in which case the time derivative term should be retained.

The reciprocal of the dimensionless offset distance from the axis of rotation, $1/x_0$ (which is identical to the ratio between the two Rayleigh numbers $Ra_\omega/Ra_{\omega 0}$) can be introduced into equation (2) to obtain

$$\left[\frac{1}{\chi}\frac{\partial}{\partial t} + 1\right]\mathbf{q} = -\nabla p - Ra_{\omega 0}\left[1 + \frac{x}{x_0}\right]T\hat{\mathbf{e}}_x \qquad (4)$$

From equation (4) it is observed that when the porous layer is far away from the axis of rotation then $x_0 \gg 1$ and the contribution of the term x/x_0 is not significant, while for a layer close enough to the rotation axis $x_0 \ll 1$ and the contribution of the first term becomes insignificant. In the first case the only controlling parameter is $Ra_{\omega 0}$ while in the latter case the only controlling parameter is $Ra_\omega = Ra_{\omega 0}/x_0$.

As all the boundaries are rigid the solution must follow the impermeability conditions there, i.e. $\mathbf{q} \cdot \hat{\mathbf{e}}_n = 0$ on the boundaries, where $\hat{\mathbf{e}}_n$ is a unit vector normal to the boundary. The temperature boundary conditions are: $T = 0$ at $x = 0$, $T = 1$ at $x = 1$ and $\nabla T \cdot \hat{\mathbf{e}}_n = 0$ on all other walls representing the insulation condition on these walls.

For convective rolls having axes parallel to the shorter dimension (i.e. y) $v = 0$, and the governing equations can be presented in terms of a stream function defined by $u = \partial\psi/\partial z$ and $w = -\partial\psi/\partial x$, which upon applying the curl $(\nabla \times)$ operator on equation (2) yields the following system of partial differential equations from equations (1), (2) and (3)

$$\left[\frac{1}{\chi}\frac{\partial}{\partial t} + 1\right]\left[\frac{\partial^2\psi}{\partial x^2} + \frac{\partial^2\psi}{\partial z^2}\right] = -[Ra_{\omega 0} + Ra_\omega x]\frac{\partial T}{\partial z} \qquad (5)$$

$$\frac{\partial T}{\partial t} + \frac{\partial\psi}{\partial z}\frac{\partial T}{\partial x} - \frac{\partial\psi}{\partial x}\frac{\partial T}{\partial z} = \frac{\partial^2 T}{\partial x^2} + \frac{\partial^2 T}{\partial z^2} \qquad (6)$$

where the boundary conditions for the stream function are $\psi = 0$ on all solid boundaries.

The set of partial differential equations (5) and (6) form a non-linear coupled system which together with the corresponding boundary conditions accepts a basic motionless conduction solution.

3. ANALYSIS

To obtain the solution to the non-linear coupled system of partial differential equations (5) and (6) we represent the stream function and temperature in the form

$$\psi = A_{11} \sin(\pi x) \sin\left(\frac{\pi z}{H}\right) \qquad (7)$$

$$T = x + B_{11} \sin(\pi x) \cos\left(\frac{\pi z}{H}\right) + B_{20} \sin(2\pi x) \qquad (8)$$

This representation is equivalent to a Galerkin expansion of the solution in both x and z directions, truncated when $i+j = 2$, where i is the Galerkin summation index in the x direction and j is the Galerkin summation index in the z direction. Substituting equations (7) and (8) into equations (5) and (6), multiplying the equations by the orthogonal eigenfunctions corresponding to equations (7) and (8) and integrating them over the domain, i.e. $\int_0^1 dx \int_0^H dz(\cdot)$, yields a set of three ordinary differential equations for the time evolution of the amplitudes, in the form

$$\frac{dA_{11}}{d\tau} = -\frac{\chi H}{\pi^2 \theta}\left[A_{11} + \frac{\xi}{\theta\pi} B_{11}\right] \qquad (9)$$

$$\frac{dB_{11}}{d\tau} = -B_{11} - \frac{1}{\pi\theta} A_{11} + \frac{1}{\theta} A_{11} B_{20} \qquad (10)$$

$$\frac{dB_{20}}{d\tau} = -\frac{1}{2\theta} A_{11} B_{11} - \frac{4H}{\theta} B_{20} \qquad (11)$$

where the time was rescaled and the following notation was introduced

$$\tau = \frac{(H^2+1)\pi^2}{H^2} t; \quad \xi = Ra_{\omega 0} + \frac{Ra_\omega}{2}; \quad \theta = \frac{H^2+1}{H} \qquad (12)$$

The fixed (i.e. stationary) points of the system of equations (9), (10) and (11) are obtained by setting all the time derivatives equal to zero and solving the resulting algebraic equations. They yield the following possible solutions

$$A_{11} = B_{11} = B_{20} = 0 \tag{13}$$

representing the motionless conduction solution and

$$A_{11} = \mp 2\sqrt{2}(H^2+1)^{1/2}\left(\frac{\xi}{\pi^2\theta^2}-1\right)^{1/2} \tag{14}$$

$$B_{11} = \pm \frac{2\sqrt{2}H\pi\theta^2}{(H^2+1)^{1/2}\xi}\left(\frac{\xi}{\pi^2\theta^2}-1\right)^{1/2} \tag{15}$$

$$B_{20} = \frac{(\xi-\pi^2\theta^2)}{\pi\xi} \tag{16}$$

representing the steady convective solutions. It is convenient to introduce the following further notation

$$R = \frac{\xi}{\pi^2\theta^2} \quad \gamma = \frac{H^2}{H^2+1} \quad \alpha = \frac{\chi\gamma}{\pi^2} \tag{17}$$

and rescale the amplitudes with respect to their convective fixed points in the form

$$X = -\frac{A_{11}}{2\theta\sqrt{2\gamma(R-1)}} \quad Y = \frac{\pi R B_{11}}{2\sqrt{2\gamma(R-1)}}$$

$$Z = \frac{\pi R B_{20}}{(R-1)} \tag{18}$$

to provide the following set of scaled equations which are equivalent to equations (9), (10) and (11)

$$\dot{X} = \alpha(Y-X) \tag{19}$$

$$\dot{Y} = RX - Y - (R-1)XZ \tag{20}$$

$$\dot{Z} = 4\gamma(XY-Z) \tag{21}$$

where the primes ($\dot{}$) denote time derivatives $\mathrm{d}(\,)/\mathrm{d}\tau$.

Equations (19), (20) and (21) are equivalent to Lorenz equations (Lorenz [16], Sparrow [17]) although with different coefficients. The demonstration of this equivalence is provided in Appendix A. However, since Lorenz equations were extensively analysed and solved for parameter values corresponding to gravity driven convection in pure fluids (i.e. non-porous domains) and even there the parameter values most frequently used correspond to $\alpha = 10$ and $\gamma = 2/3$, it is of interest to analyse and solve the corresponding equations for parameter values corresponding to the present problem under investigation.

Therefore, the fixed points of the rescaled system are $X_1 = Y_1 = Z_1 = 0$ corresponding to the motionless solution, and $X_{2,3} = \pm 1$, $Y_{2,3} = \pm 1$, $Z_{2,3} = 1$ corresponding to the convection solution.

The next step is to perform a stability analysis of the stationary solutions in order to determine the nature of the dynamics about the fixed points. The system equations (19), (20), (21) has the general form $\dot{\mathbf{X}} = \mathbf{f}(\mathbf{X})$ and the equilibrium (stationary or fixed) points $\mathbf{X}_s$ are defined by $\mathbf{f}(\mathbf{X}_s) = \mathbf{0}$. The stability matrix is established by evaluating the Jacobian $(\partial f_i/\partial X_j)_{X_s}$ at the fixed point of interest X_s. The eigenvalues of the stability matrix, evaluated by solving the zeros of the characteristic polynomial associated with the stability matrix, provide the stability conditions. A fixed point is stable if all eigenvalues corresponding to its stability matrix are negative (or in the case of complex eigenvalues they have negative real parts) and it is not stable if at least one eigenvalue becomes positive (or in the case of complex eigenvalues it has a positive real part).

The stability of the fixed point associated with the motionless solution ($X_1 = Y_1 = Z_1 = 0$) is controlled by the zeros of the following characteristic polynomial equation for the eigenvalues, λ_i ($i = 1, 2, 3$)

$$(4\gamma+\lambda)[\alpha R-(\alpha+\lambda)(1+\lambda)] = 0 \tag{22}$$

The first eigenvalue $\lambda_1 = -4\gamma$ is always negative as $\gamma > 0$. The other two eigenvalues are always real and given by $\lambda_{2,3} = [-(\alpha+1) \pm \sqrt{(\alpha+1)^2+4\alpha(R-1)}]/2$. λ_3 is also always negative and λ_2 provides the stability condition for the motionless solution in the form $\lambda_2 < 0 \Leftrightarrow R < 1$. Therefore the critical value of R, where the motionless solution loses stability and the convection solution (expressed by the other two fixed points) takes over, is obtained as $R_{c1} = R_{cr} = 1$. The significance of this result can be established by expressing it in terms of the original parameters by using equations (17) and (12), i.e. $(Ra_{\omega 0} + Ra_{\omega}/2)_{cr} = \pi^2\theta^2$. Two limiting cases of interest are (i) $x_0 \to 0$ corresponding to $Ra_{\omega 0} \to 0$ which yields $Ra_{\omega,cr} = 2\theta^2\pi^2$ and (ii) $x_0 \gg 1$ (say $x_0 \to \infty$) which yields $Ra_{\omega 0,cr} = \theta^2\pi^2$. The value of θ has to be consistent with the wavenumber at the stability threshold in order for the convection cells to fit into the domain and satisfy the boundary conditions. For case (i) the value of θ_{cr} was found by Vadasz (1996) to be $\theta_{cr} = 2.0003$ while for case (ii) $\theta_{cr} = 2$. Substituting these values yields for case (i) $Ra_{\omega,cr} = 8.0023\pi^2$ which is only 2.5% off the accurate result presented by Vadasz [9] and for case (ii) $Ra_{\omega 0,cr} = 4\pi^2$ which is the accurate result. The slight inaccuracy in the result corresponding to case (i) is due to the Galerkin truncation.

The stability of the fixed points associated with the convection solution ($X_{2,3}$, $Y_{2,3}$, $Z_{2,3}$) is controlled by the following cubic equation for the eigenvalues, λ_i ($i = 1, 2, 3$)

$$\lambda^3 + (4\gamma+\alpha+1)\lambda^2 + 4\gamma(\alpha+R)\lambda + 8\gamma\alpha(R-1) = 0 \tag{23}$$

This characteristic polynomial equation for the stability matrix eigenvalues around the convection fixed points is identical to the corresponding equations obtained from Lorenz model (Sparrow [17]) with the only difference being in the physical interpretation (and accordingly the numerical values) of the par-

ameter α, γ and R. Equation (23) yields three eigenvalues. The smallest eigenvalue λ_1 is always real and negative over all the range of parameters values. The other two are real and negative at slightly supercritical values of R, therefore the convection fixed points are stable, i.e. simple nodes. As the value of R increases these two roots move on the real axis towards the origin, the smallest between the two chasing the other one and reducing the distance between them. For $\alpha = 50/\pi^2$ and $\gamma = 0.5$ these roots become equal when $R \cong 1.28$. It is exactly at this point when these two roots become complex conjugate. However, they have still negative real parts, therefore the convection fixed points are stable, i.e. spiral nodes. As the value of R increases further, both the imaginary and real parts of these two complex conjugate eigenvalues increase and, on the complex plane, they cross the imaginary axis, i.e. their real part becomes non-negative at a value of R given by

$$R_{c2} = \frac{\alpha(\alpha+4\gamma+3)}{(\alpha-4\gamma-1)} \tag{24}$$

At this point the convection fixed points lose their stability and chaos sets in. Just prior to this happening, at the point when the complex eigenvalues cross the imaginary axis a Hopf bifurcation occurs, i.e. at R_{c2} these eigenvalues are purely imaginary leading to a limit cycle (periodic solution). The evolution of the complex eigenvalues for $\alpha = 50/\pi^2$ and $\gamma = 0.5$ is presented in Fig. 2 providing a graphical description of the sequence of events leading to the loss of stability of the convection fixed points. For $\alpha = 50/\pi^2$ and $\gamma = 0.5$ the loss of stability of the convection fixed points is evaluated using equation (24) to be $R_{c2} = 24.68$.

An interesting observation can be made by investigating the behaviour of the value of R_{c2} as α becomes very big. When $\alpha \gg 1$ the time derivative term in Darcy's equation and consequently in equation (19) is very small and this fact provides the justification of neglecting this term. By taking the limit of R_{c2} in equation (24) one obtains that $R_{c2} \to \alpha$ as $\alpha \to \infty$. Therefore although a much higher value for transition to chaos is required when the values of α are very big this transition still exists, while neglecting the time derivative term in equation (19) wipes out this possibility as the dimensionality of the system reduces to two. Of course, alternatively one could use more modes in the Galerkin expansion thus still allowing this transition to occur. However at this level of truncation including the time derivative term is necessary in order to keep all possibilities of transitions in the model.

4. METHOD OF SOLUTION

Adomian's decomposition method (Adomian [10, 11]), is applied to solve the system of equations (19), (20) and (21). The method provides in principle an analytical solution in the form of an infinite power series for each dependent variable and its excellent accuracy in solving non-linear equations was demonstrated by Olek [12, 13]. The solution follows Olek [13] and considers the following more general dynamical system of equations

$$\frac{dX_i}{dt} = \sum_{j=1}^{m} b_{ij}X_j + \sum_{l=1}^{m}\sum_{j=1}^{m} a_{ijl}X_jX_l, \quad \forall i = 1,2,\ldots,m \tag{25}$$

given the initial conditions $X_i(0)$, $i = 1,2,\ldots,m$. It can be easily observed that the system of equations (19), (20) and (21) is just a particular case of equation

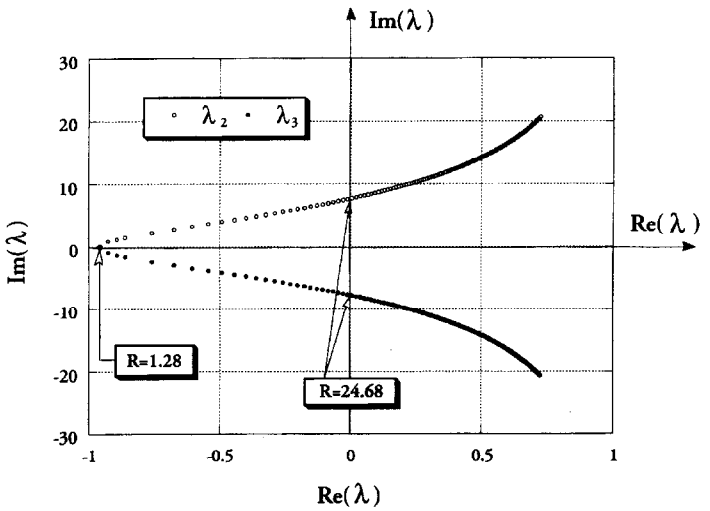

Fig. 2. The evolution of the complex eigenvalues with increasing the Rayleigh number, for $\alpha = 50/\pi^2$ and $\gamma = 0.5$.

(25). A brief description of the method of solution is provided in Appendix B.

Olek [12, 13] used the decomposition method to solve a variety of non-linear problems, some of which have closed form analytical solutions and a comparison was provided between the results obtained via the decomposition method and either exact analytical or numerical results. The conclusion from the comparison was that the decomposition method provided results which were accurate up to 14 significant digits. Even when only three terms were kept in the decomposition series solution of the Lotka–Volterra equations the results agreed by at least five significant digits with a corresponding numerical solution. The problem can actually be solved to the desired accuracy by including more terms in the computation of the series.

For the system of equation (25) the non-linear terms are of the rather simple X^2 form, so that very simple symmetry rules for the decomposition polynomials can be used. If we denote $\mathscr{L} \equiv \mathrm{d}/\mathrm{d}t$, the formal solution of equation (25) may be presented in the form

$$X_i(t) = X_i(0) + \mathscr{L}^{-1}\left[\sum_{j=1}^{m} b_{ij}X_j + \sum_{l=1}^{m}\sum_{j=1}^{m} a_{ijl}X_jX_l\right] \quad \forall i = 1,2,\ldots,m \tag{26}$$

where $\mathscr{L}^{-1} \equiv \int_0^t [\cdot]\,\mathrm{d}t$. According to the decomposition method an expansion of the following form is assumed

$$X_i(t) = \sum_{n=0}^{\infty} \tilde{X}_{in} \quad \forall i = 1,2,\ldots,m \tag{27}$$

Substituting equation (27) into equation (26) yields after rearranging the products

$$X_i(t) = X_i(0) + \mathscr{L}^{-1}\left[\sum_{j=1}^{m} b_{ij}\sum_{n=0}^{\infty}\tilde{X}_{jn} + \sum_{l=1}^{m}\sum_{j=1}^{m} a_{ijl}\sum_{n=0}^{\infty}\sum_{k=0}^{n}\tilde{X}_{jk}\tilde{X}_{l(n-k)}\right] \quad \forall i = 1,2,\ldots,m \tag{28}$$

The solution is ensured by requiring

$$\tilde{X}_{i0} = X_i(0) \quad \forall i = 1,2,\ldots,m \tag{29}$$

$$\tilde{X}_{i1} = \mathscr{L}^{-1}\left[\sum_{j=1}^{m} b_{ij}\tilde{X}_{j0} + \sum_{l=1}^{m}\sum_{j=1}^{m} a_{ijl}\sum_{k=0}^{0}\tilde{X}_{jk}\tilde{X}_{l(0-k)}\right] \quad \forall i = 1,2,\ldots,m \tag{30}$$

$$\tilde{X}_{i2} = \mathscr{L}^{-1}\left[\sum_{j=1}^{m} b_{ij}\tilde{X}_{j1} + \sum_{l=1}^{m}\sum_{j=1}^{m} a_{ijl}\sum_{k=0}^{1}\tilde{X}_{jk}\tilde{X}_{l(1-k)}\right] \quad \forall i = 1,2,\ldots,m \tag{31}$$

$$\tilde{X}_{in} = \mathscr{L}^{-1}\left[\sum_{j=1}^{m} b_{ij}\tilde{X}_{j(n-1)} + \sum_{l=1}^{m}\sum_{j=1}^{m} a_{ijl}\sum_{k=0}^{n-1}\tilde{X}_{jk}\tilde{X}_{l(n-k-1)}\right] \quad \forall i = 1,2,\ldots,m \tag{32}$$

After carrying out the integrations, the following solution is obtained

$$X_i(t) = \sum_{n=0}^{\infty} c_{in}\frac{t^n}{n!} \quad \forall i = 1,2,\ldots,m \tag{33}$$

where

$$c_{i0} = X_i(0) \quad \forall i = 1,2,\ldots,m \tag{34}$$

and the general term for $n \geqslant 1$ is defined through the following recurrence relationship

$$c_{in} = \sum_{j=1}^{m} b_{ij}c_{j(n-1)} + (n-1)!\sum_{l=1}^{m}\sum_{j=1}^{m}\sum_{k=0}^{n-1} a_{ijl}\frac{c_{jk}}{k!}\frac{c_{l(n-k-1)}}{(n-k-1)!} \quad \forall i = 1,2,\ldots,m \tag{35}$$

The decomposition method does not assure, on its own, existence and uniqueness of the solution. In fact, it can be safely applied when a fixed point theorem holds. A theorem proved by Répaci [18] indicates that there is no point in looking for solutions globally in time. On the other hand, the decomposition method can be used as an algorithm for the approximation of the dynamical response in a sequence of time intervals $[0, t_1), [t_1, t_2), \ldots, [t_{n-1}, t_n)$ such that the solution at t_p is taken as initial condition in the interval $[t_p, t_{p+1})$ which follows. This approach has the following advantages: (i) in each time-interval one can apply a theorem proved by Répaci [18], which states that the solution obtained by the decomposition method converges to a unique solution as the number of terms in the series becomes infinite, and (ii) the approximation in each interval is continuous in time and can be obtained with the desired accuracy corresponding to the desired number of terms.

The latter procedure is adopted in the computation of the solution to equations (19), (20) and (21). One can easily observe that this set of equations are just a particular case of equation (25) with $m = 3$. The set of equations (19), (20) and (21) provide the following non-zero coefficients for substitution in equation (25)

$$b_{11} = -\alpha; \quad b_{12} = \alpha; \quad b_{21} = R; \quad b_{22} = -1; \quad b_{33} = -4\gamma; \quad a_{213} = -(R-1); \quad a_{312} = 4\gamma \tag{36}$$

Except for these coefficients all others are identically zero. In all computations we used 15 terms in the series and a time interval of $\Delta\tau = 10^{-3}$.

5. RESULTS AND DISCUSSION

The method of solution presented in the previous section was applied to obtain the sets of results for different supercritical values of R. All solutions were obtained using the same initial conditions which were selected to be in the neighbourhood of the positive convective fixed point. As such the common initial conditions are at $t = 0$: $X = Y = Z = 1.1$. Since the paper's objectives are to demonstrate different possible solution results and transitions as the value of R

varies we did not make any attempt to investigate at this stage the effect of the other two parameters γ and α on the results. Except for the conclusion regarding the effect of α on the transitions when $\alpha \to \infty$, which was presented in Section 3, these two parameters were kept constant with the following values: $\gamma = 0.5$ and $\alpha = 50/\pi^2$. All computations were carried out initially up to a value of maximum time $\tau_{max} = 80$, but subsequently it was established that this was not sufficient, especially for R values in the vicinity of expected transitions. Therefore all computations have been repeated up to a maximum time of $\tau_{max} = 160$. The time step used for the computational procedure described in the previous section was constant for all cases and set to be $\Delta\tau = 10^{-3}$, while 15 terms in the series were used. The solution data points were post-processed for graphical representation of the results in the form of state space projections of trajectories onto the Y–X, Z–Y and Z–X planes.

The initial supercritical convective solutions are presented in Fig. 3 where the solution data points, which represent trajectories, were projected onto the Y–X and Z–T planes, respectively. The solution data points were not connected. From the figure it is evident that at a slightly supercritical value of R, i.e. $R = 1.1$, the convective solution is a stable simple node, i.e. the trajectory moves towards the fixed point, $X_S = Y_S = Z_S = 1$, on a straight line. For $R = 2$ the solution shows that the trajectory is attracted to the convective fixed point via a spiral, i.e. the fixed point is a stable spiral node, which is consistent with the eigenvalues analysis which predicted a transition of the two originally real roots to a pair of complex conjugate roots at a value of $R = 1.28$. At higher values of R, e.g. $R = 5$ and $R = 10$ the spiralling approach of the trajectories towards the steady state fixed point is even more pronounced, a fact which is consistent with the eigenvalues results presented in Fig. 2, indicating that the values of their imaginary parts increase as the value of R increases. The results presented in Fig. 4 indicate that as the value of R increases further to $R = 20$ the trajectory spirals so many times before it reaches the fixed point that its projection on the Y–X and Z–Y planes can be interpreted in a misleading way. Connecting the trajectory's data points does not provide a better presentation, as most of the plane is then filled black by the trajectories. This is felt in the results for $R = 23$ too, which show in addition a small white hole at the convection fixed point. This indicates that the solution needed to continue further beyond the maximum time value of $\tau_{max} = 160$ in order to fill the space very close to the fixed point. At $R = 24$ the results are even more difficult to interpret, however by observing the $X(\tau)$, $Y(\tau)$ and $Z(\tau)$ time domain patterns (which are not included here) it is evident that the solution is still heading in a spiral fashion towards the convective fixed point, however a much longer time (i.e. beyond $\tau_{max} = 160$) is needed for it to get there. At a value of $R = 24.32$ the projection of the trajectory's data points presented in Fig. 4 indicates that a limit cycle was created, i.e. the solution is not heading anymore towards the convective fixed point but rather fluctuates periodically around it. Note that the solution data points were not connected, their projection on the Y–X and Z–Y planes still forms what can be seen as a continuous curve (these are not Poincaré sections). Beyond this value of $R = 24.32$ the trajectories are neither attracted anymore to the fixed point, nor do they create a limit cycle, but rather wind around in an irregular fashion, not repeating or intersecting themselves. This regime is defined as non-periodic or chaotic. The value of $R = 24.32$ where the transition occurred via the Hopf bifurcation (i.e. the transition was preceded by a limit cycle which occurs at a particular value of R and only at this particular value) is only 1.5% off the value predicted from the eigenvalue analysis, when the real part of the pair of complex conjugate eigenvalues became positive at $R = 24.68$ and the convective fixed points lost their stability. The Hopf bifurcation associated with this transition is subcritical similarly as in the original Lorenz system corresponding to convection in pure fluids (non-porous domains). The solution results for a value of R slightly above this transition, i.e. for $R = 24.6$ are presented in Fig. 5. Figure 5(a) presents the results of the trajectory's data points projected onto the Y–X and Z–Y planes after a time of $\tau_{max} = 80$. It is evident from the figure that the results up to this time value can be easily confused and thought to be qualitatively similar to the ones presented in Fig. 4 corresponding to $R = 24$. Only an inspection of the data in the time domain, i.e. $X(\tau)$, $Y(\tau)$ and $Z(\tau)$ (which are not included here), indicated that many subsequent maxima values of $X(\tau)$, $Y(\tau)$ and $Z(\tau)$ are still growing as a function of time, suggesting to extend the maximum time to another value far beyond $\tau_{max} = 80$. When the maximum time was set to $\tau_{max} = 160$ for the same value of $R = 24.6$, we obtained the results presented in Fig. 5(b) which show that the solution is chaotic. Since the trajectory presented here includes all the transient evolution one can magnify the figure obtained for the chaotic solution, Fig. 5(b), around the fixed convective point, and present it in the form shown in Fig. 5(c). Now, the comparison between Figs. 5(c) and 5(a) shows that evidently Fig. 5(a) is only a partial picture of the more developed chaotic solution presented in Fig. 5(b). The projection of the trajectory onto the Y–X, Z–X and Z–Y planes at a value of $R = 26$ is presented in Figs. 6, 7 and 8, respectively. In these figures the evolution of the trajectory over the transient is excluded. While Figs. 6(b), 7(b) and 8(b) represent the corresponding projections of the solution data points onto the Y–X, Z–X and Z–Y planes, respectively, the same corresponding projections while connecting the data points are presented in Figs. 6(a), 7(a) and 8(a). Note that the trajectory does not intersect itself if we consider the full three-dimensional picture. The crossings in Figs. 6(a), 7(a) and 8(a) are the results of the pro-

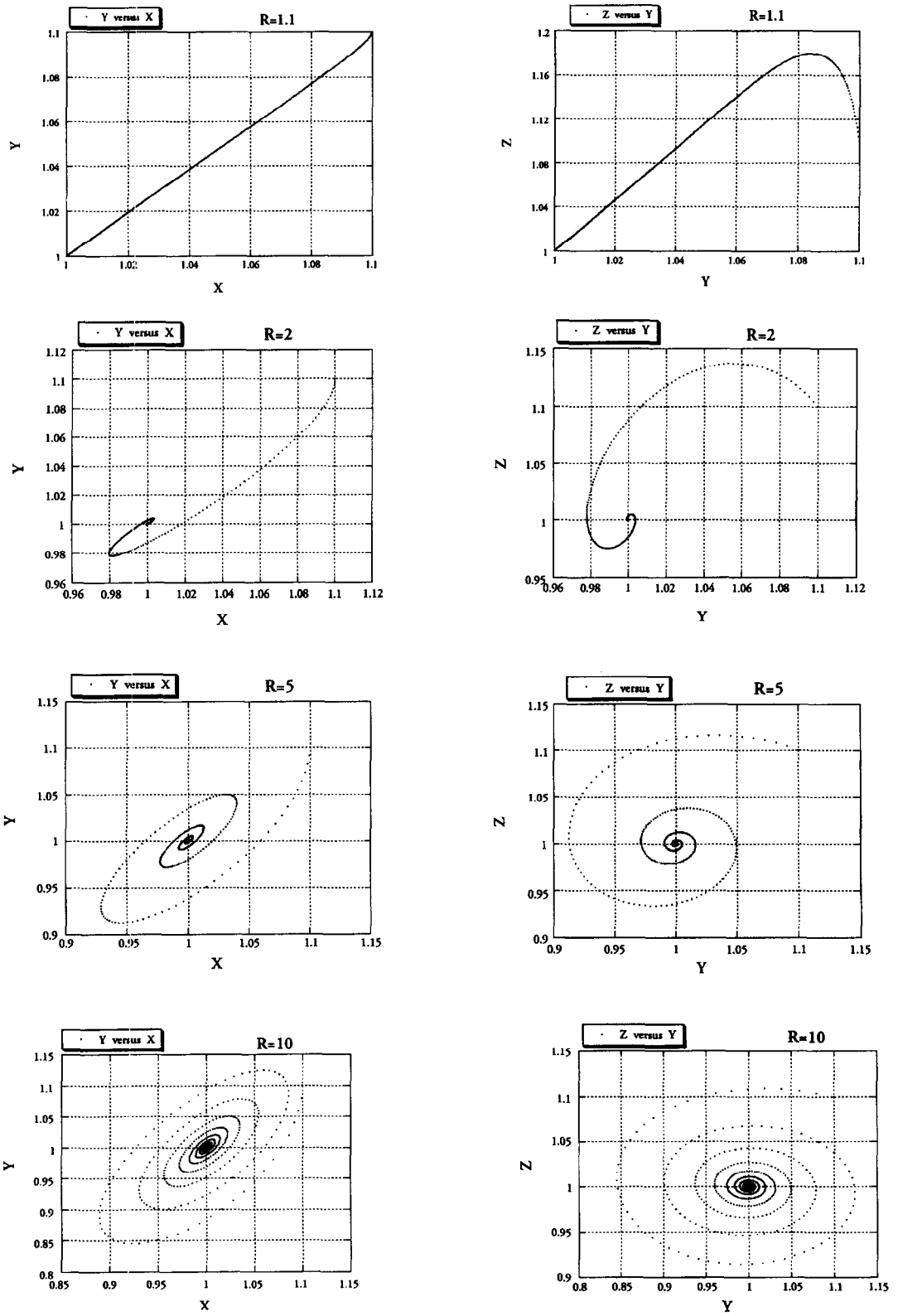

Fig. 3. The evolution of trajectories over time in the state space for increasing values of Rayleigh number (in terms of R) corresponding to $R \geqslant 1.1$ and $R \leqslant 10$. The graphs represent the projection of the solution data points onto the Y–X and Z–Y planes, respectively.

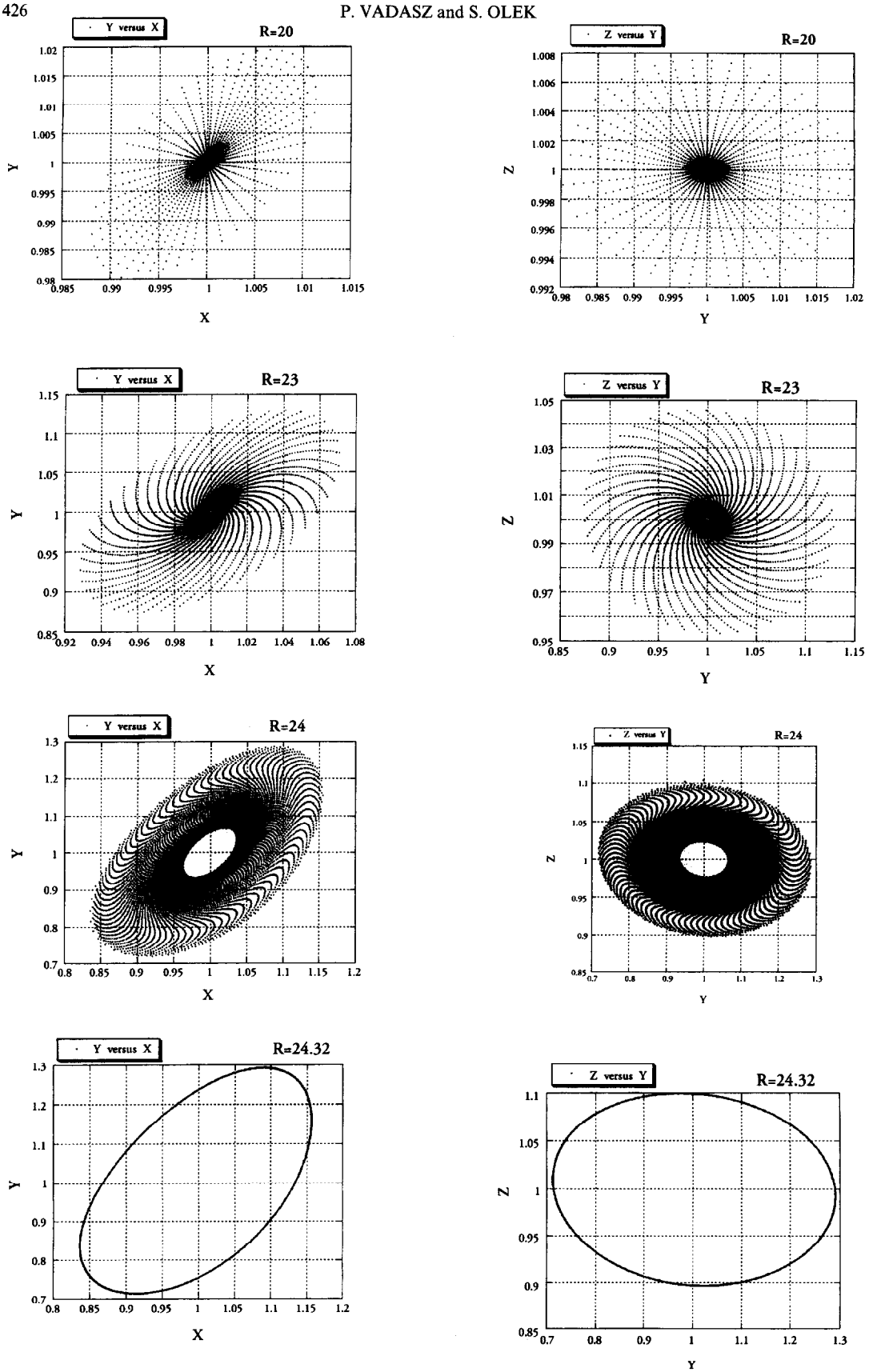

Fig. 4. The evolution of trajectories over time in the state space for increasing values of Rayleigh number (in terms of R) corresponding to $R \geqslant 20$ and $R \leqslant 24.32$. The graphs represent the projection of the solution data points onto the Y–X and Z–Y planes, respectively.

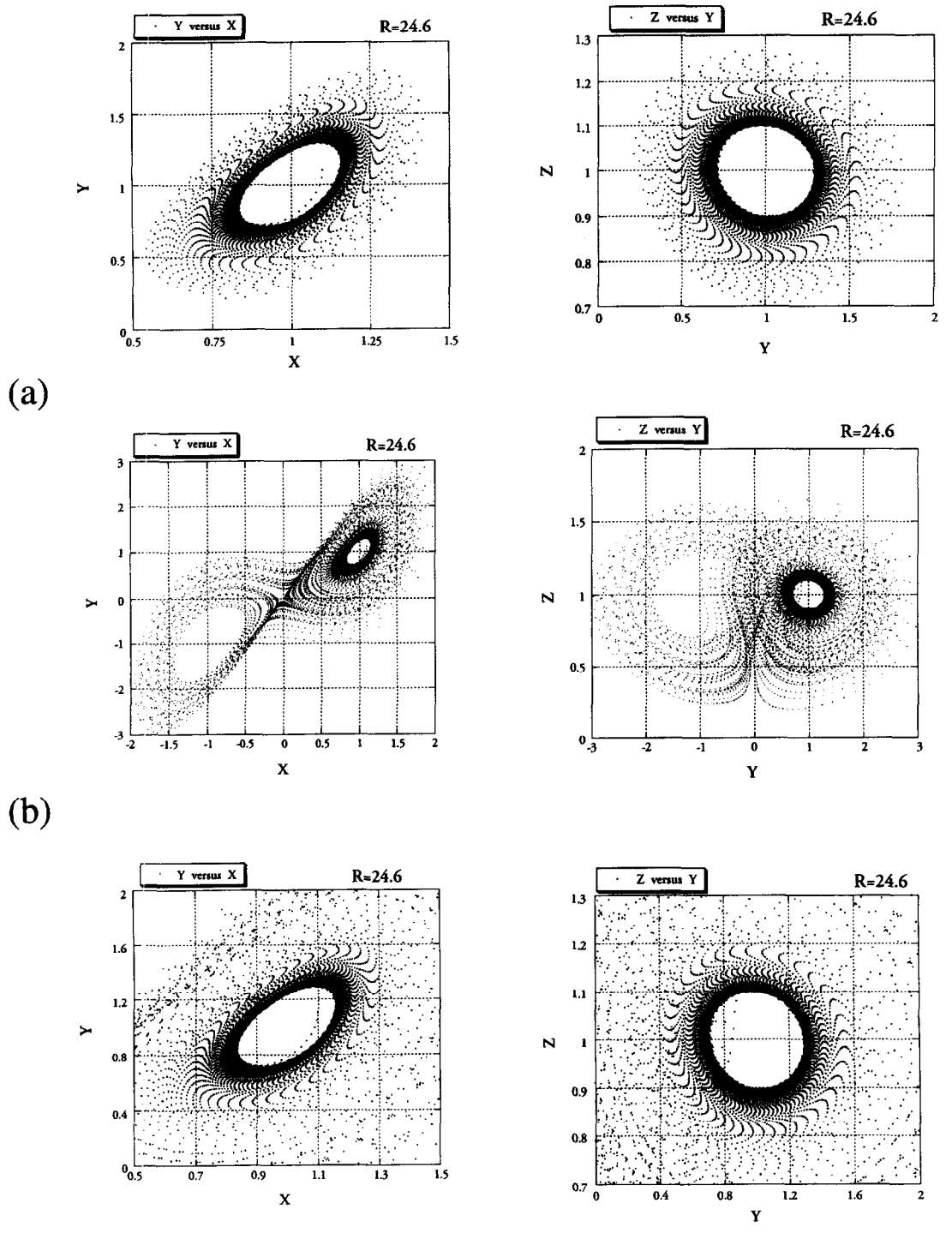

Fig. 5. The evolution of trajectories over time in the state space for a value of Rayleigh number (in terms of R) just beyond the transition to a non-periodic regime, corresponding to $R = 24.6$. The graphs represent the projection of the solution data points onto the Y–X and Z–Y planes, respectively. (a) Results up to $\tau = 80$, (b) results up to $\tau = 160$, (c) results up to $\tau = 160$ magnified around the fixed point $X = Y = Z = 1$.

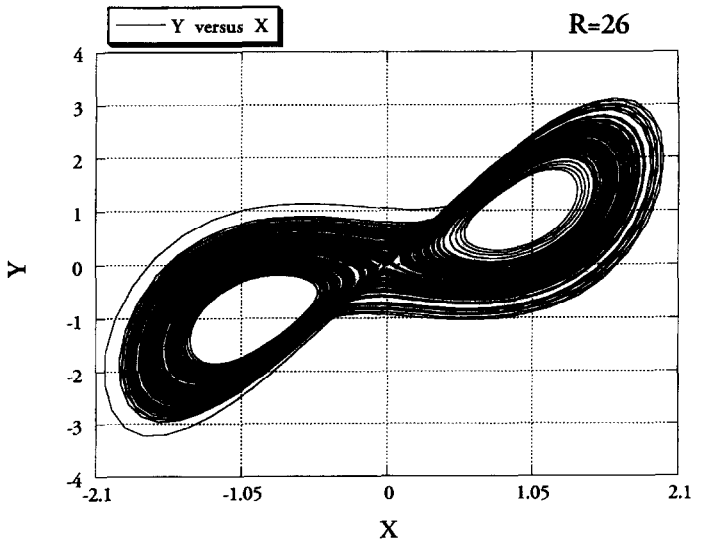

(a)

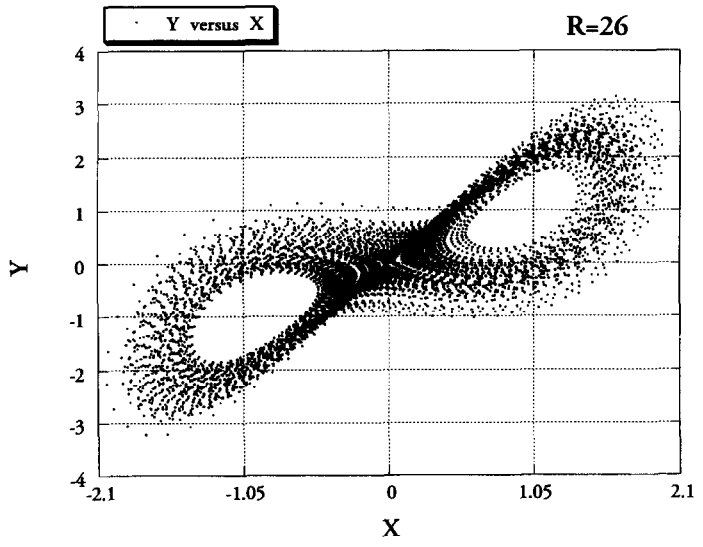

(b)

Fig. 6. The evolution of trajectories over time in the state space for a value of Rayleigh number (in terms of R) corresponding to $R = 26$. Initial transient values not included. (a) The projection of trajectories onto the Y–X plane by connecting the solution data points. (b) The projection of the solution data points (not connected) onto the Y–X plane.

jection of the results onto two dimensions. A plot of successive maxima of Z plotted against each other for $R = 26$ is presented in Fig. 9 providing a confirmation of the chaotic regime. The results of higher values of R indicate qualitatively similar chaotic features, however a slightly different pattern starts showing up for values of R close to $R = 75$. The post transient trajectory's data points projected onto the Y–X, Z–X and Z–Y planes at $R = 75$ are presented in Fig. 10, where this slightly different pattern can be observed. At a further higher value of R, slightly above $R \cong 100$ a transition from chaos to a periodic solution is obtained which persists over a wide range of values of R. We performed our computations up to $R = 250$ where the periodic solution was still obtained. The trajectory's data points projected onto the Y–X, Z–X and Z–Y planes, corresponding to $R = 250$ are presented in Fig. 11 indicating the projection of the limit

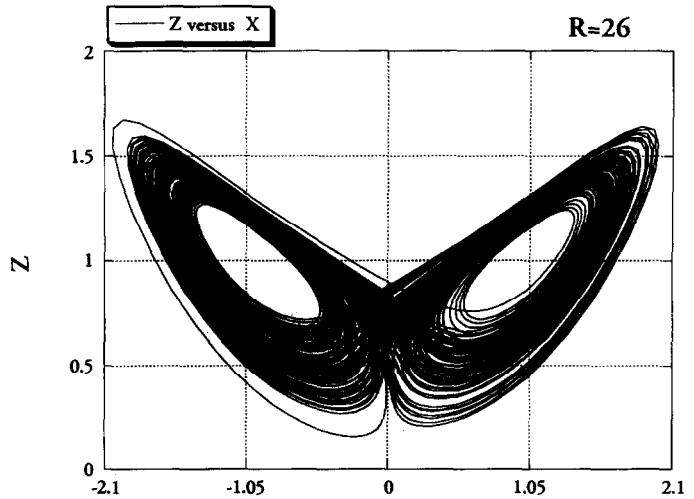

(a)

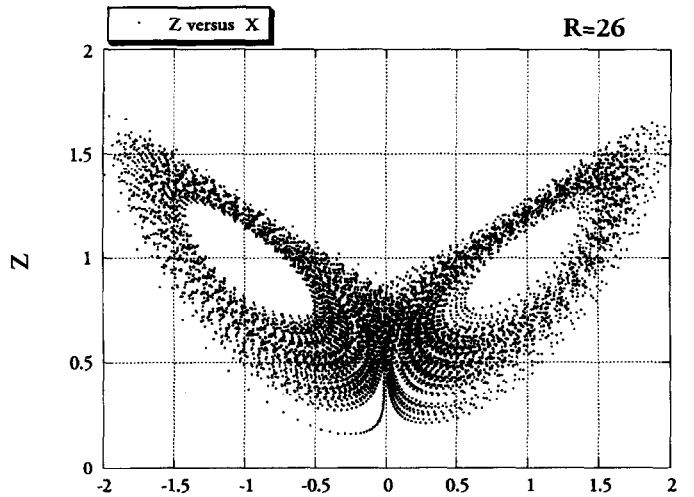

(b)

Fig. 7. The evolution of trajectories over time in the state space for a value of Rayleigh number (in terms of R) corresponding to $R = 26$. Initial transient values not included. (a) The projection of trajectories onto the Z–X plane by connecting the solution data points. (b) The projection of the solution data points (not connected) onto the Z–X plane.

cycle. Note that the solution data points in Fig. 11 were not connected, their projection onto the corresponding planes still forms what can be seen as a continuous curve (these are not Poincaré sections). It should be pointed out that Sparrow [17] shows analytically the existence of periodic solutions to Lorenz equations for large values of R for the corresponding problem of convection in pure fluids (non-porous domains).

With the solution for the stream function and temperature completed at different values of R one can evaluate the average (in time as well as in space) rate of heat transfer in terms of an average Nusselt number defined in the form

$$\overline{Nu} = \frac{1}{H(\tau_1 - \tau_0)} \int_{\tau_0}^{\tau_1} d\tau \int_0^H dz \left(\frac{\partial T}{\partial x}\right)_{x=0} \tag{37}$$

where $(\tau_1 - \tau_0)$ is the time interval over which the time

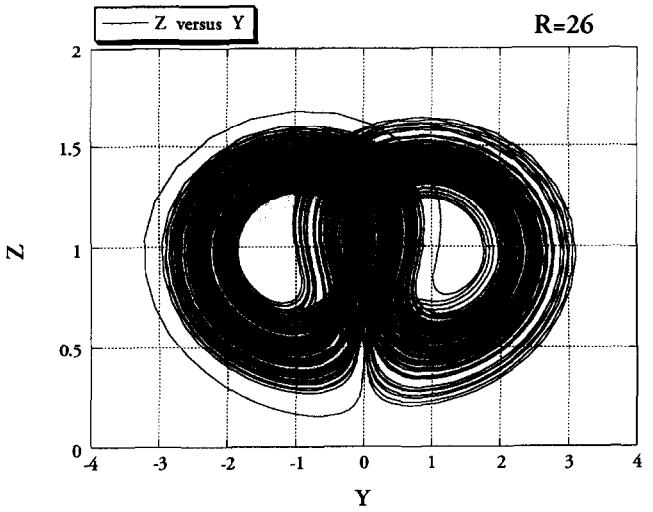

(a)

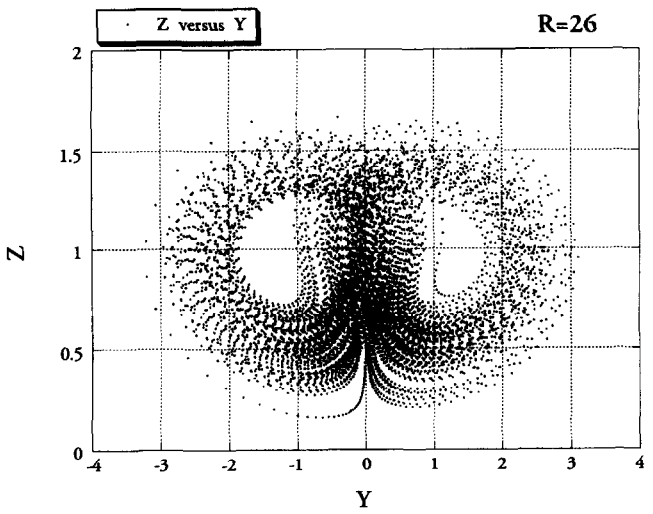

(b)

Fig. 8. The evolution of trajectories over time in the state space for a value of Rayleigh number (in terms of R) corresponding to $R = 26$. Initial transient values not included. (a) The projection of trajectories onto the Z–Y plane by connecting the solution data points. (b) The projection of the solution data points (not connected) onto the Z–Y plane.

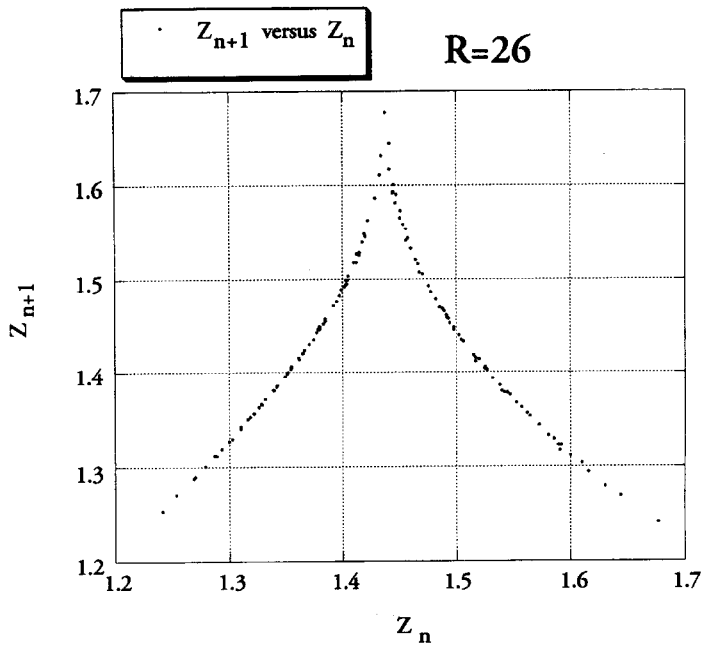

Fig. 9. Successive maxima of Z plotted against each other for $R = 26$.

average is sought. Substituting equation (8) and the notation adopted through equation (18) and equation (37) yields the following expression for the average Nusselt number

$$\overline{Nu} = 1 + \frac{2(R-1)}{R(\tau_1 - \tau_0)} \int_{\tau_0}^{\tau_1} Z \, d\tau \qquad (38)$$

The solution for $Z(\tau)$ as obtained at different values of R was introduced in equation (38), while including post-transient values of the solution only, i.e. values of $Z(\tau)$ after allowing the transient to fade away. Therefore the lower limit of the integrals in equations (37) and (38), τ_0, represents the time when no more transient effects are felt, and the upper limit $\tau_1 = \tau_{max}$. The results of this procedure, while the integration was performed numerically, were plotted as a function of R and are presented in Fig. 12, where the data points represent the numerical results obtained. From the figure it can be observed that the average Nusselt number initially increases as the value of R increases beyond the critical value for convection, however a sudden reduction in the average heat transfer is associated with the transition from steady to non-periodic convection followed by a partial recovery as the value of R increases further. A slight change of pattern of the curve $Nu(R)$ is observed at a value of R when transition from chaos to a periodic regime occurs, i.e. at a value slightly over $R \cong 100$. There, it seems that the derivative, $d\,Nu/dR$, of the curve is not continuous.

6. CONCLUSIONS

The non-linear problem of centrifugally driven free convection in a rotating porous layer was solved for a truncated Galerkin approximation. At this level of truncation it was demonstrated that the set of non-linear ordinary differential equations are equivalent to Lorenz equations although with different coefficients. An algorithm employing the Adomian decomposition method was used to solve the equations thus providing a semi-analytical solution. The results demonstrate different transitions, e.g. from steady convection to a non-periodic regime via a Hopf bifurcation, and a further transition from chaos to periodic convection at significantly higher values of the centrifugal Rayleigh number. The first transition is confirmed by a stability analysis of the steady convection. These transitions show a marked impact on the average heat transfer. All the reservations which are applicable to Lorenz model are of course applicable here as well and developing a model which includes more Galerkin modes is indeed required for improving the accuracy and confidence regarding the different transitions and in particular at the higher values of the centrifugal Rayleigh number. Nevertheless, useful information can be drawn at the present rank of approximation which can be applied when investigating the problem at a higher rank.

Acknowledgement—One of the authors wishes to thank the Foundation for Research Development (South African) for partially supporting this study through the Competitive Industry Research Grant (CIPM-GUN2034039).

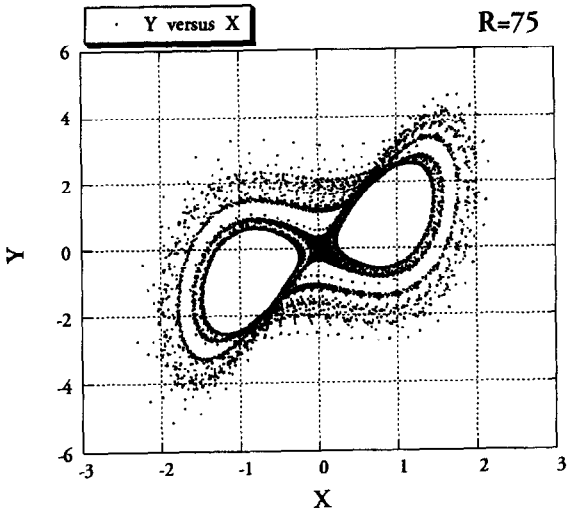

(a)

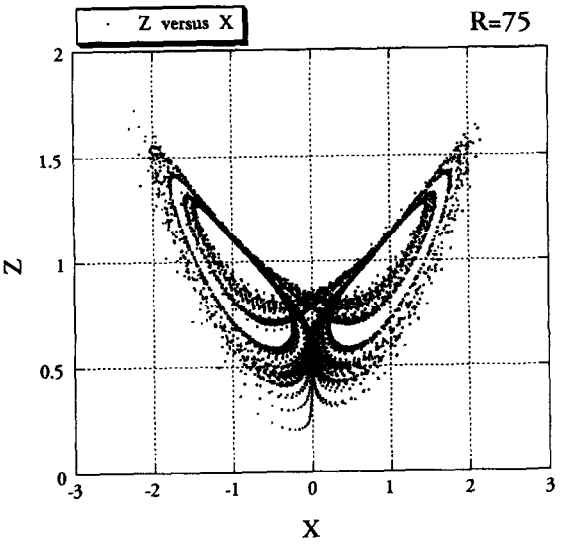

(b)

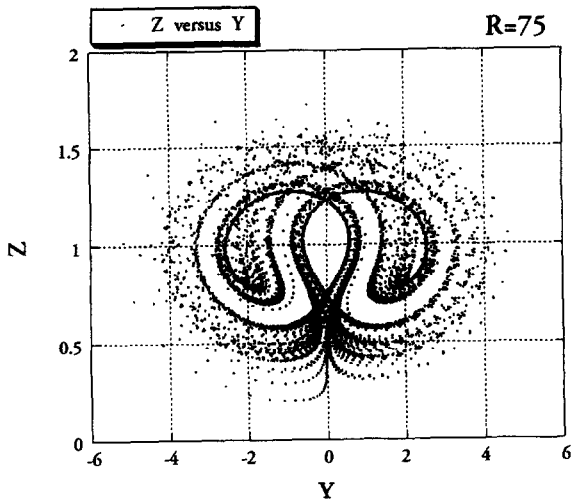

(c)

Fig. 10. The evolution of trajectories over time in the state space for a value of Rayleigh number (in terms of R) corresponding to $R = 75$. Initial transient values not included. (a) The graphs represent the projection of the solution data points onto the (a) Y–X plane, (b) Z–X plane and (c) Z–Y plane.

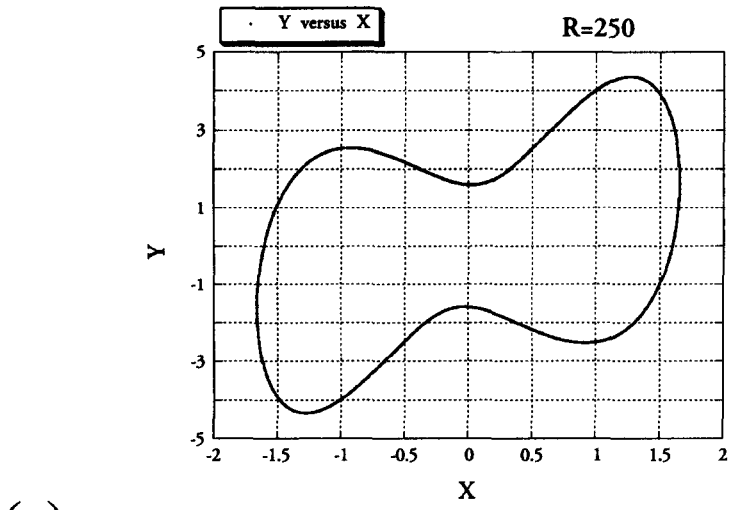

(a)

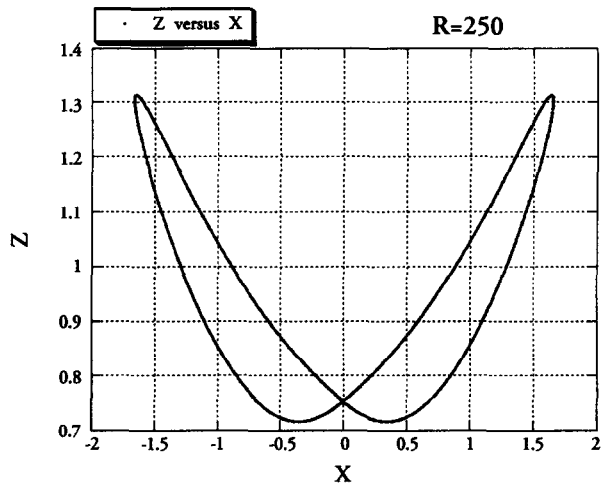

(b)

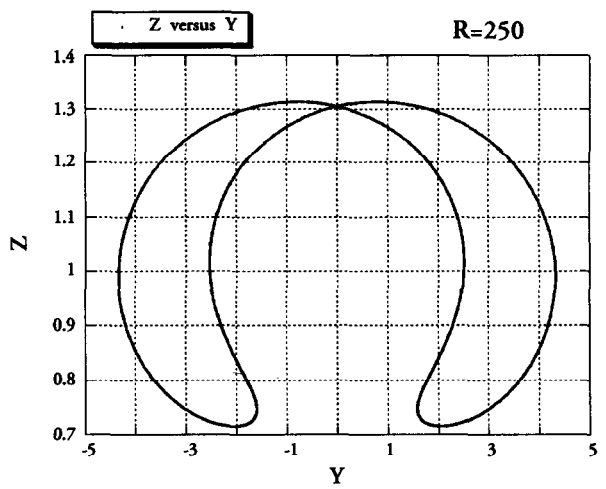

(c)

Fig. 11. The evolution of trajectories over time in the state space for a value of Rayleigh number (in terms of R) corresponding to $R = 250$. Initial transient values not included. The graphs represent the projection of the solution data points (not connected) onto the (a) Y–X plane, (b) Z–X plane and (c) Z–Y plane.

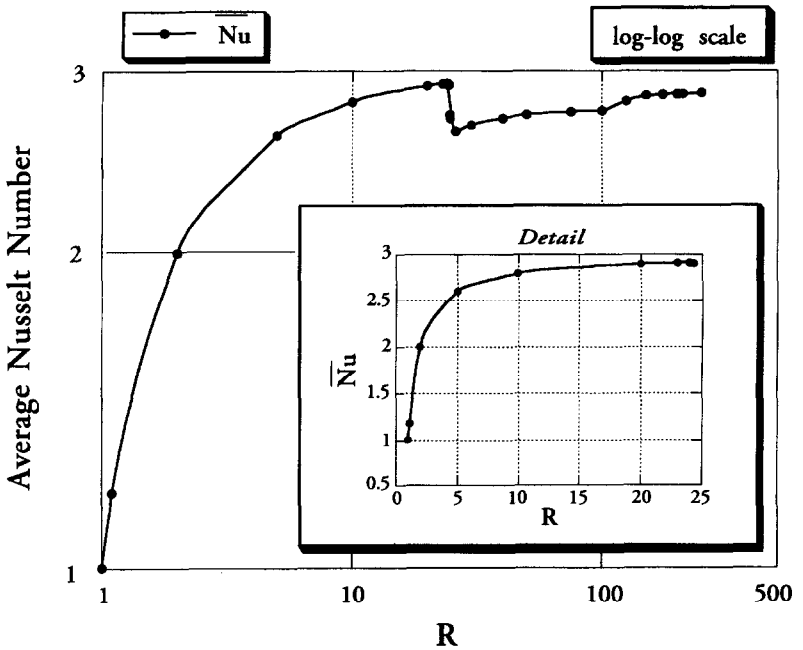

Fig. 12. The time and space average heat transfer in terms of Nusselt number as a function of Rayleigh number (in terms of R).

REFERENCES

1. Nield, D. A. and Bejan, A., *Convection in Porous Media.* Springer Verlag, New York, 1992.
2. Bejan, A., *Convection Heat Transfer*, 2nd edn. Wiley, New York, 1995.
3. Patil, P. R. and Vaidyanathan, G., On setting up of convection currents in a rotating porous medium under the influence of variable viscosity. *International Journal of Engineering Science*, 1983, **21**, 123–130.
4. Jou, J. J. and Liaw, J. S., Transient thermal convection in a rotating porous medium confined between two rigid boundaries. *International Communication in Heat and Mass Transfer*, 1987, **14**, 147–153.
5. Jou, J. J. and Liaw, J. S., Thermal convection in a porous medium subject to transient heating and rotation. *International Journal of Heat and Mass Transfer*, 1987, **30**, 208–211.
6. Rudraiah, N., Shivakumara, I. S. and Friedrich, R., The effect of rotation on linear and non-linear double-diffusive convection in sparsely packed porous medium. *International Journal of Heat and Mass Transfer*, 1986, **29**(9), 1301–1317.
7. Palm, E. and Tyvand, A., Thermal convection in a rotating porous layer. *Journal of Applied Mathematics and Physics (ZAMP)*, 1984, **35**, 122–123.
8. Vadasz, P., Three-dimensional free convection in a long rotating porous box. *Journal of Heat Transfer*, 1993, **115**, 639–644.
9. Vadasz, P., Stability of free convection in a rotating porous layer distance from the axis rotation. *Transport in Porous Media*, 1996, **23**, 153–173.
10. Adomian, G., *Solving Frontier Problems in Physics: The Decomposition Method.* Kluwer Academic Publisher, Dordrecht, 1994.
11. Adomian, G., A review of the decomposition method in applied mathematics. *J. Math. Anal. Appl.*, 1988, **135**, 501–544.
12. Olek, S., An accurate solution to the multispecies Lotka–Volterra equations. *SIAM Review*, 1994, **36**, 480–488.
13. Olek, S., Solution to a class of nonlinear evolution equations by Adomian's decomposition method. Manuscript in preparation, 1997.
14. Govender, S., Stability analysis of free convection in rotating porous media subject to centrifugal and gravitational body forces. M.Sc. thesis, University of Durban-Westville, 1995.
15. Dagan, G., Some aspects of heat and mass transfer in porous media. In *Fundamentals of Transport Phenomena in Porous Media.* Elsevier, 1972.
16. Lorenz, E. N., Deterministic non-periodic flows. *J. Atmos. Sci.*, 1963, **20**, 130–141.
17. Sparrow, C., *The Lorenz Equations: Bifurcations, Chaos, and Strange Attractors.* Springer-Verlag, New York, 1982.
18. Répaci, A., Non-linear dynamical systems: on the accuracy of Adomian's decomposition method. *Appl. Math. Lett.*, 1990, **3**, 35–39.

APPENDIX A

The objective of this appendix is to demonstrate that the system of equations (19), (20) and (21) is equivalent to Lorenz equations (Lorenz [16]). We start with Lorenz equations as presented by Sparrow [17] in the form

$$\dot{X} = \sigma(Y - X) \tag{A1}$$

$$\dot{Y} = rX - Y - XZ \tag{A2}$$

$$\dot{Z} = XY - bZ \tag{A3}$$

Its fixed convection points are $(X_s, Y_s, Z_s) = (\pm[b(r-1)]^{1/2}, \pm[b(r-1)]^{1/2}, (r-1))$. Scaling the variables with respect to these fixed points in the form

$$\tilde{X} = \frac{X}{[b(r-1)]^{1/2}} \quad \tilde{Y} = \frac{Y}{[b(r-1)]^{1/2}} \quad \tilde{Z} = \frac{Z}{(r-1)} \tag{A4}$$

transforms equations (A1), (A2) and (A3) to the following form

$$\dot{\tilde{X}} = \sigma(\tilde{Y} - \tilde{X}) \tag{A5}$$

$$\dot{\tilde{Y}} = r\tilde{X} - \tilde{Y} - (r-1)\tilde{X}\tilde{Z} \tag{A6}$$

$$\dot{\tilde{Z}} = b(\tilde{X}\tilde{Y} - \tilde{Z}) \tag{A7}$$

Equations (A5), (A6) and (A7) are identical to equations (19), (20) and (21) derived in the main body of the paper with the following equivalence of parameters $\sigma \to \alpha$, $r \to R$ and $b \to 4\gamma$. The physical significance of the parameters is certainly different.

APPENDIX B

The decomposition method (Adomian [10, 11]) invokes even more general equations of the form

$$\mathscr{L}X + \mathscr{R}X + \mathscr{N}X = g \tag{B1}$$

where $\mathscr{L}$ is an easily invertible linear differential operator (such as the highest order derivative), $\mathscr{R}$ is the remainder of the linear differential operator, $\mathscr{N}X$ represents the non-linear terms, and g denotes the non-homogeneous part. Solving for $\mathscr{L}X$ yields

$$\mathscr{L}X = g - \mathscr{R}X - \mathscr{N}X \tag{B2}$$

Because $\mathscr{L}$ is invertible, an expression equivalent to equation (B2) is

$$\mathscr{L}^{-1}\mathscr{L}X = \mathscr{L}^{-1}g - \mathscr{L}^{-1}\mathscr{R}X - \mathscr{L}^{-1}\mathscr{N}X \tag{B3}$$

In the case of an initial-value problem, the integral operator $\mathscr{L}^{-1}$ may be regarded as definite integrals from t_0 to t. If $\mathscr{L}$ is a first order operator, $\mathscr{L}^{-1}$ is an one-fold integration operator and $\mathscr{L}^{-1}\mathscr{L}X = X - X(t_0)$. Solving equation (B2) for X yields

$$X = X(t_0) + \mathscr{L}^{-1}g - \mathscr{L}^{-1}\mathscr{R}X - \mathscr{L}^{-1}\mathscr{N}X \tag{B4}$$

The non-linear term $\mathscr{N}X$ will be equated to $\Sigma_{n=0}^{\infty} C_n$, where the C_n are special polynomials to be discussed, and X will be decomposed into $\Sigma_{n=0}^{\infty} X_n$, with X_0 identified as $X(t_0) + \mathscr{L}^{-1}g$, so that

$$\sum_{n=0}^{\infty} X_n = X_0 - \mathscr{L}^{-1}\mathscr{R}\sum_{n=0}^{\infty} X_n - \mathscr{L}^{-1}\sum_{n=0}^{\infty} C_n \tag{B5}$$

Consequently, we can write

$$X_1 = -\mathscr{L}^{-1}\mathscr{R}X_0 - \mathscr{L}^{-1}C_0 \tag{B6}$$

$$X_2 = -\mathscr{L}^{-1}\mathscr{R}X_1 - \mathscr{L}^{-1}C_1 \tag{B7}$$

$$X_{n+1} = -\mathscr{L}^{-1}\mathscr{R}X_n - \mathscr{L}^{-1}C_n \tag{B8}$$

The polynomials C_n are generated for each particular non-linearity so that C_0 depends only on X_0, C_1 depends only on X_0 and X_1, C_2 depends only on X_0, X_1 and X_2, etc. All of the C_n components are calculable, and $X = \Sigma_{n=0}^{\infty} X_n$. If the series converges, the n-term partial sum $S_n = \Sigma_{j=0}^{n-1} X_j$ will be the approximate solution since $\lim_{n\to\infty} S_n = \Sigma_{j=0}^{\infty} X_j = X$ by definition. It is important to emphasise that the C_n can be calculated for complicated nonlinearities of the form $f(X, X', \ldots)$ or $f(g(X))$. The C_n polynomials are defined by

$$C_0 = f(X_0) \tag{B9}$$

$$C_1 = X_1 \frac{\mathrm{d}f(X_0)}{\mathrm{d}X_0} \tag{B10}$$

$$C_2 = X_2 \frac{\mathrm{d}f(X_0)}{\mathrm{d}X_0} + \frac{X_1^2}{2!}\frac{\mathrm{d}^2 f(X_0)}{\mathrm{d}X_0^2} \tag{B11}$$

$$C_3 = X_3 \frac{\mathrm{d}f(X_0)}{\mathrm{d}X_0} + X_1 X_2 \frac{\mathrm{d}^2 f(X_0)}{\mathrm{d}X_0^2} + \frac{X_1^3}{3!}\frac{\mathrm{d}^3 f(X_0)}{\mathrm{d}X_0^3} \tag{B12}$$

There are a number of ways to define the general term C_n. One form is

$$C_n = \frac{1}{n!}\sum_{v=1}^{n} c(v, n)\frac{\mathrm{d}^v f}{\mathrm{d}X^v} \tag{B13}$$

where the second index in the coefficient is the order of the derivative and the first index progresses from 1 to n along with the order of the derivative. In the linear case $f(X) = X$ and the polynomials C_n reduce to X_n. Otherwise $C_n = C_n(X_0, X_1, \ldots, X_n)$. For $f(X) = X^2$, for example, $C_0 = X_0^2$, $C_1 = 2X_0X_1$, $C_2 = X_1^2 + 2X_0X_2$, $C_3 = 2X_1X_2 + 2X_0X_3, \ldots$, etc. It is to be noted that in this scheme, the sum of the subscripts in each term of the C_n is equal to n. It is possible to find simple symmetry rules for writing the C_n quickly to higher orders.